Optimization of Suture-Free Laser-Assisted Vessel Repair by Solder-Doped Electrospun Poly(ε-caprolactone) Scaffold

Dara R. Pabittei,[1,2] Michal Heger,[3] Johan F. Beek,[4] Sjoerd van Tuijl,[5] Marc Simonet,[6] Allard C. van der Wal,[7] Bas A. de Mol,[1,5,6] and Ron Balm[2]

[1]Department of Cardiothoracic Surgery, Academic Medical Center, University of Amsterdam, Meibergdreef 9, 1105 AZ Amsterdam, The Netherlands; [2]Department of Surgery, Academic Medical Center, University of Amsterdam, Meibergdreef 9, 1105 AZ Amsterdam, The Netherlands; [3]Department of Experimental Surgery, Academic Medical Center, University of Amsterdam, Meibergdreef 9, 1105 AZ Amsterdam, The Netherlands; [4]Department of Biomedical Engineering and Physics, Academic Medical Center, University of Amsterdam, Meibergdreef 9, 1105 AZ Amsterdam, The Netherlands; [5]HemoLab, Den Dolech 2, 5612 AZ Eindhoven, The Netherlands; [6]Department of Biomedical Engineering, Technical University Eindhoven, PO Box 513, 5600 MB Eindhoven, The Netherlands; and [7]Department of Pathology, Academic Medical Center, University of Amsterdam, Meibergdreef 9, 1105 AZ Amsterdam, The Netherlands

Associate Editor Jane Grande-Allen oversaw the review of this article.

Abstract—Poor welding strength constitutes an obstacle in the clinical employment of laser-assisted vascular repair (LAVR) and anastomosis. We therefore investigated the feasibility of using electrospun poly(ε-caprolactone) (PCL) scaffold as reinforcement material in LAVR of medium-sized vessels. *In vitro* solder-doped scaffold LAVR (ssLAVR) was performed on porcine carotid arteries or abdominal aortas using a 670-nm diode laser, a solder composed of 50% bovine serum albumin and 0.5% methylene blue, and electrospun PCL scaffolds. The correlation between leaking point pressures (LPPs) and arterial diameter, the extent of thermal damage, structural and mechanical alterations of the scaffold following ssLAVR, and the weak point were investigated. A strong negative correlation existed between LPP and vessel diameter, albeit LPP (484 ± 111 mmHg) remained well above pathophysiological pressures. Histological analysis revealed that thermal damage extended into the medial layer with a well-preserved internal elastic lamina and endothelial cells. Laser irradiation of PCL fibers and coagulation of solder material resulted in a strong and stiff scaffold. The weak point of the ssLAVR modality was predominantly characterized by cohesive failure. In conclusion, ssLAVR produced supraphysiological LPPs and limited tissue damage. Despite heat-induced structural/mechanical alterations of the scaffold, PCL is a suitable polymer for weld reinforcement in medium-sized vessel ssLAVR.

Keywords—Adhesive and cohesive strength, Anastomosis, Medium-sized vessels, Polymeric biomaterial, Tissue welding.

Address correspondence to Ron Balm, Department of Surgery, Academic Medical Center, University of Amsterdam, Meibergdreef 9, 1105 AZ Amsterdam, The Netherlands. Electronic mail: R.Balm@amc.uva.nl

INTRODUCTION

In contrast to conventional suture anastomoses, the advantages of using laser energy for end-to-end and end-to-side vascular coaptations include the elimination of needle trauma and suture materials,[12] the reduction of foreign body reaction,[7] immediate liquid-tight sealant, and the possibility of a faster and easier procedure for minimally invasive and endoscopic anastomotic techniques.[3,22,33] Despite these advantages, limited welding strength, extensive collateral thermal damage, poor reproducibility, and ambiguous end-points[3] comprise the drawbacks that have delayed the clinical application of laser-assisted vascular anastomoses/repair (LAVA/R), particularly in medium-sized vessels.

Recent studies have focused on biodegradable polymer scaffolds as reinforcement material in solder-mediated LAVA/R (sLAVA/R) to optimize welding strength for medium-sized vessels.[6,19,20,25–27] In light of these trends, electrospun poly(ε-caprolactone) (PCL) has been introduced as reinforcement material for liquid sLAVR *in vitro*. Scaffolds composed of microfiber-based PCL mesh were shown to increase welding strength by 2.8-fold vs. sLAVR, obtaining a mean ± SD leaking point pressure (LPP) of 749 ± 171 mmHg.[23] In contrast to the most commonly used polymer for scaffold-enforced sLAVR (ssLAVR), namely, poly(DL-lactic acid-*co*-glycolic-acid) (PLGA), the slow degradation kinetics of PCL have been associated with a greater biocompatibility.[28] Furthermore,

the mean LPP obtained with electrospun PCL ssLAVR was significantly higher than the mean LPP of 300 mmHg obtained using scaffolds composed of PLGA and polyethylene glycol.[19] In a previous study, Bregy *et al.* reported a significant improvement in breaking strength using solvent-casting-particulate-leached PCL scaffold in ssLAVR of rabbit abdominal aortas,[6] demonstrating additional advantages of PCL vs. other polymeric scaffold materials for ssLAVR.

In a previous study[23] we established the optimum parameters for electrospun PCL ssLAVR, namely, a mean scaffold thickness of 187 μm composed of 14-μm thick fibers in combination with a liquid solder containing 50% bovine serum albumin (BSA) and 0.5% methylene blue (MB) and an irradiance of 5.8 W/cm^2 administered over two consecutive passes, using LPP as the outcome parameter. To further optimize the PCL ssLAVR modality and to lay a foundation for future *in vivo* work, we have divided the current study into four specific substudies. Substudy I investigated the correlation between the vessel external diameter and acute LPPs. Subsequently, substudy II focused on the extent of thermal damage produced by laser irradiation employing the previously determined optimum ssLAVR parameters. Laser-induced alterations in PCL fiber structure and mechanical properties following welding were analyzed in substudy III. Finally, since welding strength is critically dependent on the cross-linking between albumin molecules (cohesive strength) and the cross-linking between albumin and adventitial collagens (adhesive strength), the final study (substudy IV) investigated the weak point (i.e., cohesive vs. adhesive failure) of the weld.

MATERIALS AND METHODS

Solder and Tissue Preparation

Liquid solder was prepared by dissolving 50% (w/v, final concentration) BSA (Fraction V, Sigma–Aldrich, St. Louis, MO) and 0.5% (w/v, final concentration) MB (Sigma–Aldrich) in MilliQ water at 37 °C under continuous stirring. The solder solution was stored at 4 °C in the dark until further use for up to 20 days.

Porcine carotid arteries ($n = 27$) and abdominal aortas ($n = 5$) were harvested at the slaughterhouse. Perivascular tissue was trimmed and the arteries were stored in histidine–tryptophan–ketoglutarate organ preservation solution (Custodiol, Tramedico, Weesp, The Netherlands) at 4 °C. For thermal damage assays, ssLAVR was performed on the same day. For the other experiments, the vessels were used within 3 days.

Preparation of Poly(ε-caprolactone) Scaffolds

First, PCL (Sigma–Aldrich) with an average molecular weight of 80 kDa was dissolved in chloroform under gentle stirring to obtain a 17% (w/w) solution. The polymer-containing solution was delivered at a constant flow rate (60 μL/min) to a metal capillary connected to a high-voltage power supply. The distance between the capillary and the target drum (25×120 mm) was set to 15 cm. As the jet fluid accelerated toward a grounded collector, the solvent evaporated and a charged polymer fiber was deposited on the rotating target in the form of a non-woven mesh.[2,24] Electrospinning was performed at 15 kV for 25 min to produce a mesh consisting of 14-μm diameter fibers.[23] Fiber diameter was confirmed by scanning electron microscopy (SEM) (Quanta 600F ESEM-FEG, FEI Company, Hillsboro, OR) using analytic software (Xt Microscope Control, FEI Company). Scaffolds were punched out of the mesh in a 20×4 mm array (substudies I and II), a 20×5 mm array (substudy III), and in a 5×5 mm array (substudy IV). Scaffold thickness was measured with a digital micrometer between two glass slides; the mean $\pm$ SD thickness was 200 ± 10 μm.

Experimental Design

For substudy I, ssLAVR was performed on 4-cm carotid artery segments ($n = 16$). The external diameter was measured using a digital caliper and a 10.0 ± 0.5-mm longitudinal arteriotomy was created with a scalpel and scissors. Before application of the scaffold, the opposing ends of the incised artery were aligned with tweezers without the use of stay sutures. Solder and scaffold were applied by distributing approximately 30 μL of solder over the incision site, after which the scaffold was positioned on top of the solder with the coarse surface facing the solder–tissue interface.[27] Subsequently, an additional amount of solder was uniformly distributed over the edges of the scaffold. Coaptations were irradiated as described in "Laser Irradiation" section. The strength of the weld was defined as the LPP and measured directly after the ssLAVR procedure as detailed in "Leaking Point Pressure Determination" section. Values were normalized to the respective vessel diameter. To demonstrate the correlation between vessel diameter and LPP beyond the original vessel diameter range, additional experiments were performed with arteries with an external diameter between 0.57 and 0.70 cm ($n = 4$).

In substudy II, ssLAVR was performed on intact arteries ($n = 5$) to investigate the extent of thermal damage to the vessel wall. Histological sections were stained as explained in "Thermal Damage Analysis"

section. The non-irradiated arteries ($n = 3$) were used as control.

In substudy III, ssLAVR-induced alterations in scaffold physical properties were analyzed mechanically and structurally. The mechanical properties were determined by E-modulus, yield strength, and ultimate strength. The alterations in scaffold structure were analyzed by SEM. Twenty-eight scaffolds were prepared for mechanical testing. Native electrospun PCL scaffolds were mechanically tested without any modification as control ($n = 7$). Solder-soaked scaffolds ($n = 7$) were prepared by soaking scaffolds in 1 mL of solder dispersed over a small area in a petri dish. Scaffolds were gently dabbed to enhance solder penetration. Scaffolds in the third group ($n = 7$) underwent a similar solder-soaking procedure after which they were subjected to dual-pass irradiation with a diode laser (see "Laser Irradiation" section). In the fourth group ($n = 7$), we investigated the effect of heating on PCL scaffold alone (without albumin solder). To facilitate the absorption of laser energy in the scaffolds, scaffolds were submersed for ~2 min in chromophore-containing solution (0.5% (w/v) MB in water) prior to dual-pass laser irradiation. Mechanical tests on scaffolds were performed on a tensiometer (see "Mechanical Testing and Weak Point Analysis" section). A similar procedure was performed on eight scaffolds ($n = 2$/group) for SEM analysis.

In substudy IV, the type of welding strength (i.e., cohesive vs. adhesive strength) was investigated with respect to the welding protocol. Aorta segments were cut along the longitudinal axis and 30×5 mm strips were excised from the unfolded slab of vascular tissue. The thickness of the aorta strip was measured with a digital micrometer between two glass slides. Before ssLAVR, the aorta strip was pinned to a silicone rubber (Sylgard 184, Dow Corning, Midland, MI) covered petri dish with its adventitia surface facing upward and cut into half along the longer axis. The opposing ends were realigned after which solder and PCL scaffold (5×5 mm) were applied over the incised strip, and ssLAVR was performed ($n = 10$) in accordance with "Laser Irradiation" section. The control group ($n = 10$) consisted of dual-pass sLAVR. Welding strength in this substudy was defined as breaking strength (BS) and measured directly after the welding procedures as explained in "Mechanical Testing and Weak Point Analysis" section.

Laser Irradiation

A 670-nm diode laser (model HPD7401, High Power Devices, North Brunswick, NJ) was used in continuous wave mode with a red HeNe aiming beam. The incident laser power was 0.73 W with a spot size of 12.6 mm^2, accounting for an irradiance of 5.81 W/cm^2. A fiber optic hand piece was used to deliver the laser beam perpendicularly to the scaffold surface in a single continuous pass. For substudies I and II, coaptations were lased in a gradually narrowing rectangular movement, starting at the outer margins of the weld and scanning inward, whereas for substudies III and IV the scaffold and coaptations were lased in a zigzag movement starting at the upper left corner.[34] The scan speed was dictated by MB transiting into its leucoform, i.e., irradiation of the subsequent scaffold volume was performed only after the prior scaffold area had turned white. This lasing regime was standardly applied twice per scaffold. The cumulative irradiation time was recorded for each procedure.

Leaking Point Pressure Determination

LPPs were measured in accordance with the method of Basu et al.[4] and Fahner et al.[9] One end of the laser-treated carotid segment was sealed by ligation, and the vessel lumen was filled with 0.9% saline solution containing MB as a visual indicator at 99 mL/h. The other end was ligated around a hollow needle that was connected to a rate-controlled syringe infusion pump and a pressure controller (Braun Medical, Melsungen, Germany) through an interposed T-valve. For online pressure recording, the pressure controller was coupled to a pressure transducer (Baxter Healthcare, Deerfield, IL) that transmitted the digitized output signals to a PC.

Upon complete submersion of the artery in a 0.9% saline bath, the intraluminal pressure was gradually raised by the infusion of MB-containing 0.9% saline at 99 mL/h. The LPP was defined as the pressure at which leakage was observed, which was always accompanied by a simultaneous drop in pressure.

Furthermore, to prove the consistency of the weld strength, the maximum wall tension that the weld could bear before failure was calculated from the LPPs. The wall tension (T) at the place of the weld is defined as $T = (P \times r)/h$ (according to the LaPlace law), where $P = $ LPP, $r = d/2$, and h is the thickness of the weld (constant for all welds). Plotting these wall tensions at their respective bursting pressure for each sample gave insight into the consistency of weld quality.

Thermal Damage Analysis

Histological samples were prepared from native ($n = 3$) and ssLAVR-treated ($n = 5$) carotid arteries. Immediately after ssLAVR, vessel segments were fixed in 4% buffered formalin, dehydrated in ethanol, cleared in methyl benzoate and benzene, and impregnated with paraffin wax. Of each sample, 8-μm sections

were stained with hematoxylin and eosin (H&E) and Masson's trichrome (MT) for light microscopy, and picrosirius red (PR) for polarization microscopy. Images were acquired with a Zeiss Axio microscope (Carl Zeiss, Oberkochen, Germany) equipped with a polarizer and analyzer and a CCD camera. Customized software (Zeiss Axio Imager D, Carl Zeiss) was used for image acquisition and processing and to determine the extent of vessel wall shrinkage following ssLAVR.

Scanning Electron Microscopy

The native, solder-soaked, irradiated solder-soaked, MB-soaked, and irradiated MB-soaked PCL scaffolds were viewed under SEM without prior fixation and coating. To eliminate residual water, scaffolds were kept under vacuum overnight after preparation and before SEM. The scaffold strip was cut in a 5×5 mm array and mounted to a metal stump before placement inside the SEM. Scaffolds were viewed under low vacuum at an accelerating voltage of 10 kV.

Mechanical Testing and Weak Point Analysis

Mechanical tests were performed on scaffolds (substudy III, $n = 7$/group) and on ssLAVR- and sLAVR-treated aortas (substudy IV, $n = 10$/group). The tests were performed after every five consecutive lasing procedures. Between the lasing procedures and mechanical testing, the soldered aorta strips were kept moist in phosphate buffered saline-soaked gauzes.

In substudy III, the scaffolds were mounted on a tensiometer at a grip-to-grip separation of 5 mm, and the test was performed at a test speed of 10 mm/min. *E*-modulus (MPa), yield strength (MPa), and ultimate strength (MPa) were measured to determine ssLAVR-induced alterations in scaffold mechanical properties.

In substudy IV, the ssLAVR-treated aorta strips were mounted between the metal clamps of a tensiometer (Zwick, Ulm, Germany). The distance between the grips was 10 mm. Breaking tests were performed at a test speed of 10 mm/min. Breaking strength (BS) was defined as the force (N) required to completely tear two halves of the strip divided by the cross-sectional area of the scaffold and solder (cm^2). The BS of the sLAVRed aortas was used as control. The type of dissociation during the BS measurement, assessed visually, served as an indication of the weak point of the weld (i.e., cohesive vs. adhesive failure).

Statistical Analysis

Means, standard deviations, Mann–Whitney *U* tests, and nonparametric correlation analyses were performed in GraphPad Prism (GraphPad Software, La Jolla, CA). A single asterisk (*) designates a *p*-value of ≤ 0.05 throughout the text, (**) designates a *p*-value of ≤ 0.01, and (***) designates a *p*-value of ≤ 0.001. Values are reported as mean ± SD.

RESULTS

Substudy I: Correlation Between Vessel Diameter and Acute LPPs

To determine whether a relationship existed between the arterial diameter and LPP, arteries with external diameters ranging from 0.37 to 0.57 cm were ssLAVR-treated and the LPPs were measured. Subsequently, correlation analysis was performed on the data set.

The time to complete dual-pass irradiation for each weld was 388 ± 47 s, yielding an LPP of 531 ± 59 mmHg (range of 424–634 mmHg). Figure 1a shows the LPP plotted vs. arterial external diameter. The LPPs decreased significantly with increasing vessel diameter (Spearman's $\rho = -0.72$**). Figure 1b shows the maximum wall tension plotted for each sample, exhibiting a constant quality of the weld.

Four arteries with an external diameter of 0.57–0.70 cm were added to assess the effect of the LaPlace law in the context of LPP and vessel diameter. This resulted in an increased negative correlation between vessel diameter and LPP (Spearman's $\rho = -0.85$***) and a reduction in mean LPP to 484 ± 111 mmHg (245–634 mmHg range) (Fig. 1c). Figure 1d shows that the quality of the weld remained constant after the addition of larger-diameter vessels.

Substudy II: Thermal Damage Analysis

Representative histological images of thermal damage in ssLAVR-treated arteries are presented in Fig. 2. An MT stain was used to determine laser-induced structural alterations in connective tissue (collagen stains light blue, damaged collagen stains dark blue-to-purple, and solder, elastin, and muscle fibers stain red). ssLAVR resulted in marked shrinkage of the vascular wall. Morphometrically, the wall thickness was reduced to $31 \pm 4\%$ of its original thickness (Fig. 2a). In all the cases, the thermal damage extended beyond the adventitia into the medial layer (Figs. 2a and 2b), regardless of the differences in vessel size. The scanning movement from outside–inward resulted in confined thermal damage at the outer margins of the weld to almost full thickness thermal damage at the center of the irradiated area
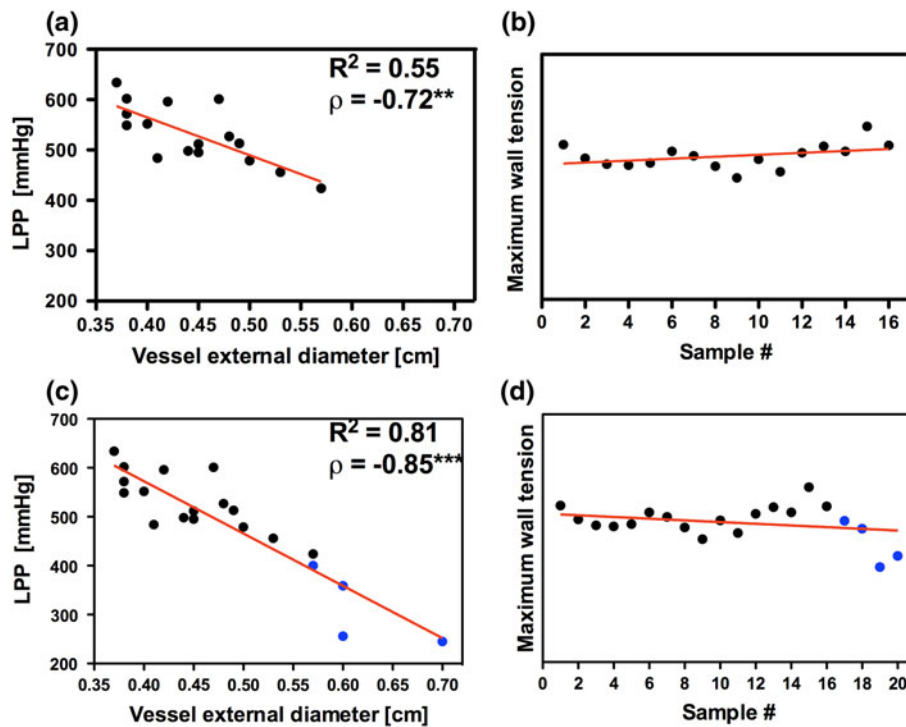
FIGURE 1. (a) A plot of LPPs vs. arterial external diameter. The data set was fitted with a linear curve fit and analyzed by nonparametric correlation analysis. The goodness of fit (R^2) and Spearman's correlation coefficient (ρ) are indicated in the upper right corner. (b) A plot of maximum wall tension per sample (n = 16). (c) A plot of LPP vs. arterial external diameter with the additional four arteries, indicated by the blue dots. The data set was fitted with a linear curve fit and analyzed by nonparametric correlation analysis. The goodness of fit (R^2) and Spearman's correlation coefficient (ρ) are indicated in the upper right corner. (d) A plot of maximum wall tension per sample (n = 20).

(Fig. 2b). At higher magnification, the thermally damaged artery (Fig. 2d) was enveloped by denatured solder (black arrowhead) that had coalesced with the homogenized and swollen adventitial collagen (arrows). Elastin fibers, on the other hand, had remained intact (Figs. 2d vs. 2c, arrowheads). Thermal damage in the media was characterized by shrinkage and an almost complete disappearance of smooth muscle cells, which resulted in a relative increase in collagen density (Fig. 2d, encircled). In contrast to the adventitial collagen, collagen in the medial layer had retained a preserved fibrillar structure (Fig. 2d).

H&E-stained sections were used to assess the morphology of the internal elastic lamina and the endothelial lining of the vessel. No notable differences were found between the irradiated and non-irradiated zones (Figs. 2e and 2f).

Polarized light microscopy of PR-stained sections showed a more homogenized and compacted structure of thermally damaged adventitial collagen (Fig. 2h). At these sites, the media showed almost complete disappearance of green birefringent collagen fibrils, indicating loss of type III collagen (rectangular marquee in Fig. 2h).

Substudy III: SEM Analysis and Mechanical Testing

Stress-to-strain curves of (a) native, (b) solder-soaked, (c) irradiated solder-soaked, and (d) irradiated MB-soaked scaffolds are depicted in Fig. 3. The embedded charts present E-modulus, yield, and ultimate strength for each group. Immersion of scaffold in solder solution did not induce notable alterations in mechanical properties. The E-modulus, yield strength, and ultimate strength of the native and solder-soaked scaffolds were 5.78 ± 2.06 MPa vs. 13.34 ± 10.12 MPa (p = 0.64), 0.56 ± 0.39 MPa vs. 0.32 ± 0.40 MPa (p = 0.34), and 1.99 ± 0.13 MPa vs. 2.04 ± 0.40 MPa (p = 0.71), respectively.

Dual-pass laser irradiation of the solder-soaked scaffold significantly decreased scaffold elasticity and markedly increased yield and ultimate strength. The E-modulus increased to 316.07 ± 89.41 MPa (** vs. native scaffold) while the yield and ultimate strength increased to 3.12 ± 0.79 MPa (** vs. native) and 4.56 ± 0.95 MPa (** vs. native), respectively.

The effect of laser irradiation alone on the physical properties of PCL scaffolds was demonstrated in the last group. Macroscopically, dual-pass laser
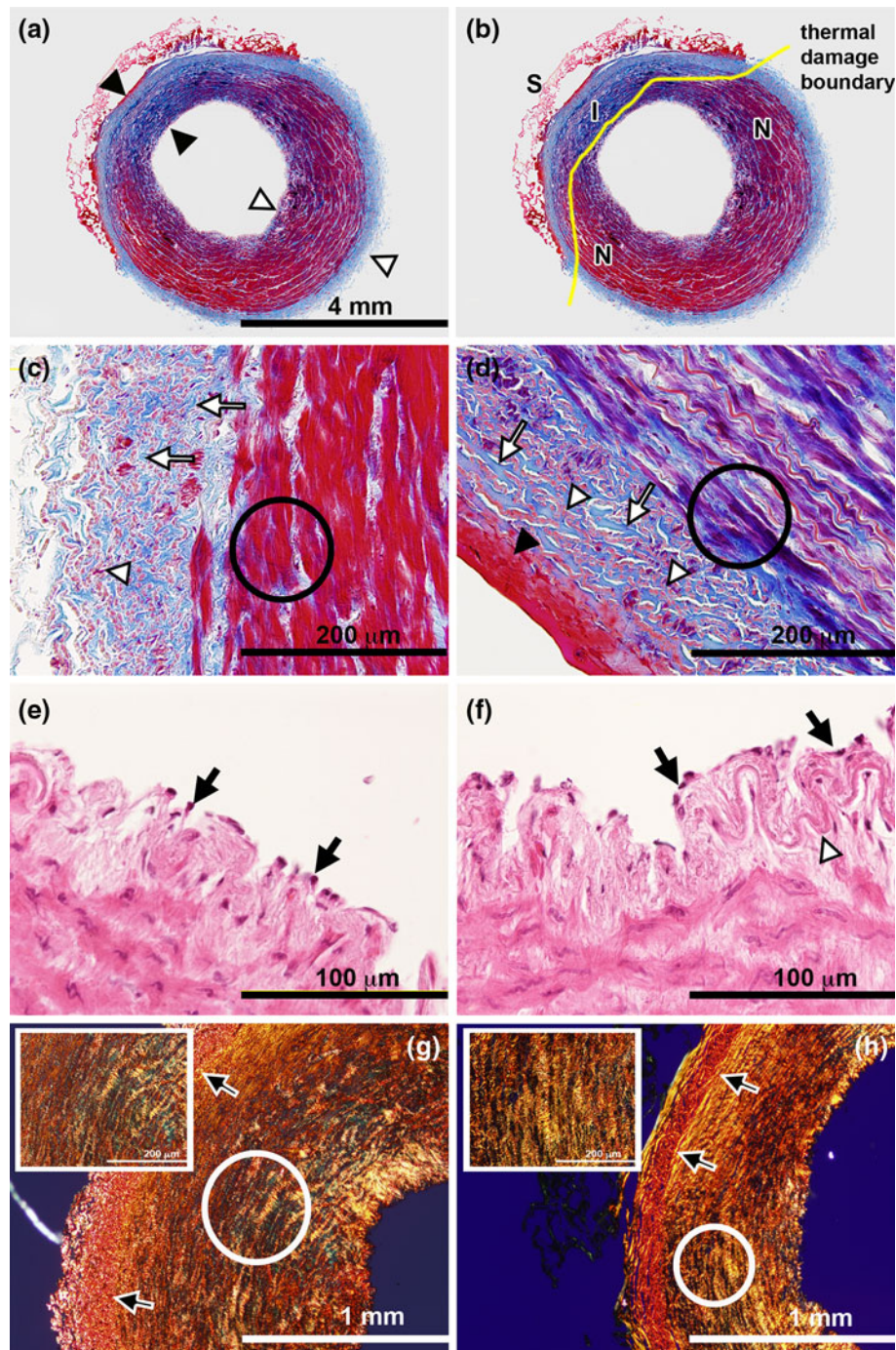
FIGURE 2. Photomicrograph of native and ssLAVR-treated arteries. (a) MT-stained section showing a reduced vessel thickness in the irradiated area (distance between black arrowheads vs. distance between white arrowheads). (b) The thermal damage is limited to the area under the solder and scaffold (S). The yellow line indicates the thermal damage boundary between the non-irradiated normal area (N) and the irradiated area (I). (c) The native artery was characterized by the loosely arranged collagen (arrow) and intact smooth muscle cells in the media (encircled), whereas the thermally damaged artery (d) shows homogenized and compacted collagen and shrunken smooth muscle cells. Hematoxylin and eosin-stained sections showing morphologically similar aspects of endothelium (black arrow) and intact lamina elastica interna (white arrowhead) in both a native (e) and ssLAVR-treated artery (f). (g) Picrosirius red (PR)-stained control artery showing collagen with intact birefringence in the adventitia (arrow) and media (encircled), as opposed to the ssLAVR-treated artery that exhibited a loss of collagen birefringence in the adventitia (arrow). Higher magnification images of the encircled areas (inserts) showed green birefringence of collagen type III in native media (g) in contrast to the almost complete loss of type III collagen in the ssLAVR-treated artery (h).
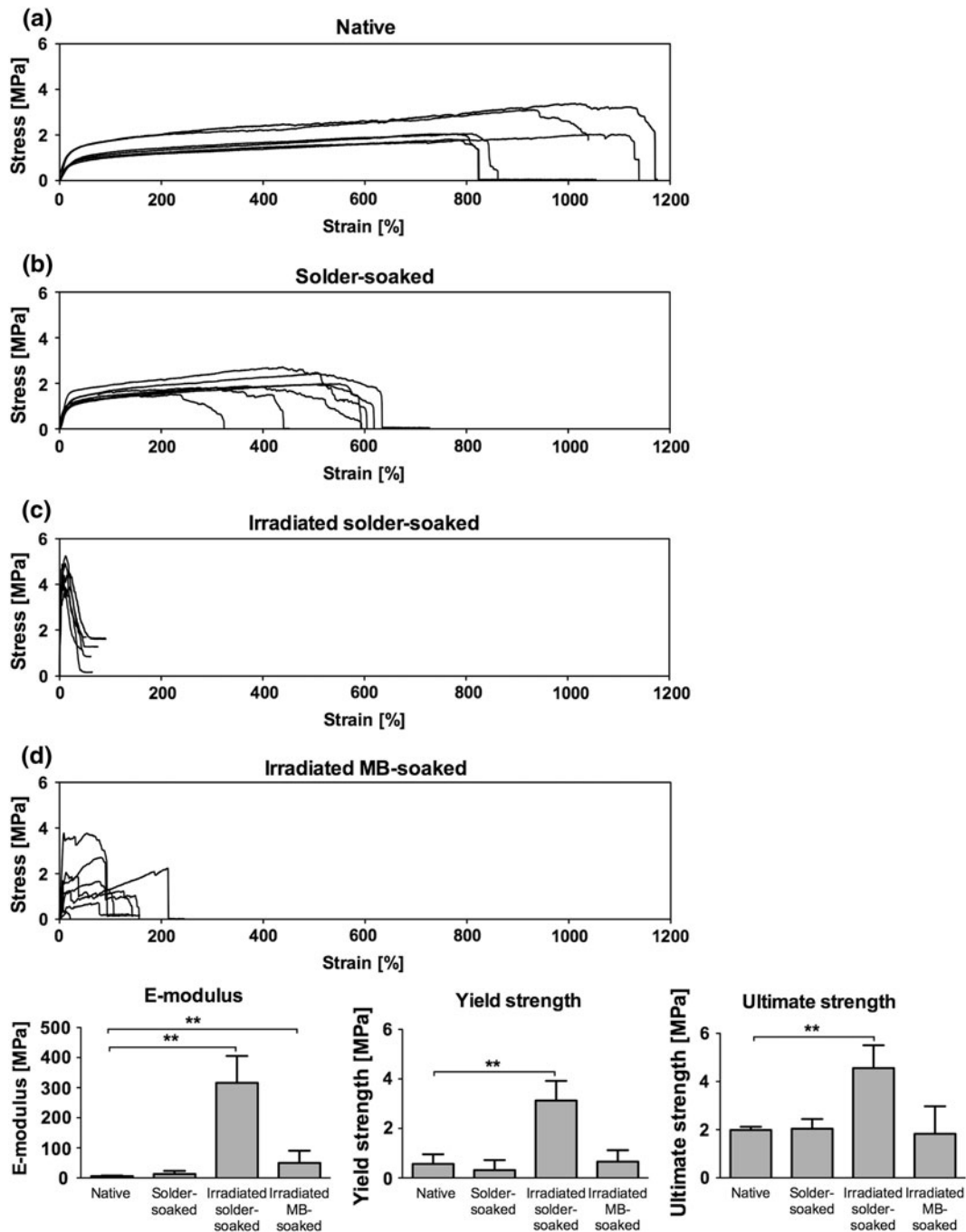
FIGURE 3. Strain-to-stress curves of the (a) control, (b) solder-soaked, (c) irradiated solder-soaked, and (d) irradiated MB-soaked scaffolds with associated mechanical properties: E-modulus (bottom left panel), yield strength (bottom middle panel), and ultimate strength (bottom right panel).

irradiation decreased scaffold width to approximately 66%, which was in stark contrast to the 4% decrease in scaffold width in the irradiated solder-soaked group. Scaffold shrinkage was accompanied by a decrease in scaffold elasticity as evidenced by the increase in E-modulus to 49.62 ± 40.80 MPa (** vs. native). Despite the shrinkage and the increase in scaffold stiffness, the irradiated fibers retained

their yield strength and ultimate strength, namely, 0.65 ± 0.47 MPa ($p = 0.41$ vs. native) and 1.85 ± 1.07 MPa, ($p = 0.35$ vs. native), respectively. The strain–stress curve of the irradiated MB-soaked scaffolds evinced that, despite the structural alterations, the fibers retained their mechanical strength and did not brake simultaneously (Fig. 3d). A drop in the trace signifies breakage of a portion of the

fibers, whereas a subsequent increase in the trace is attributable to sustained strength by the residual intact fibers.

Figure 4 presents SEM images of the native, solder-soaked, irradiated solder-soaked, and irradiated MB-soaked scaffold. The SEM image of the solder-soaked scaffold shows a solder layer between intertwined intact fibers (Fig. 4b). Dual-pass laser irradiation resulted in coagulated albumin solder that coalesced with the PCL fibers (Fig. 4c). Alterations of PCL fibers due to laser irradiation were evident in the SEM image of the irradiated MB-soaked scaffold (Fig. 4d.2), where the PCL fibers appeared melted and deteriorated.

Substudy IV: Breaking Strength and Weak Point Analysis

The time required to weld aorta strips by ssLAVR was not significantly different from the time required to coapt aorta strips by sLAVR, namely,

92 ± 11 s and 85 ± 7 s, respectively. Figure 5a shows that the BS in the sLAVR and ssLAVR groups were 50.23 ± 16.21 N/cm^2 and 104.12 ± 19.68 N/cm^2 (***), respectively.

Figure 5b illustrates the two types of failure observed during BS measurements. In cohesive failures, the coagulated solder fractured at the incision line with the solder remaining attached to the tissue surface. In adhesive failures, the coagulated solder (and scaffold) remained intact, but the welded strips failed by a partial or complete detachment of scaffold and solder from the tissue surface. In contrast to the predominantly cohesive failures (10/10) that occurred in the sLAVR group, coaptations in the ssLAVR group underwent solely adhesive failures (10/10) during mechanical testing.

DISCUSSION

In their review on laser tissue welding, Bass *et al.*[3] posited that, due to low welding strength and
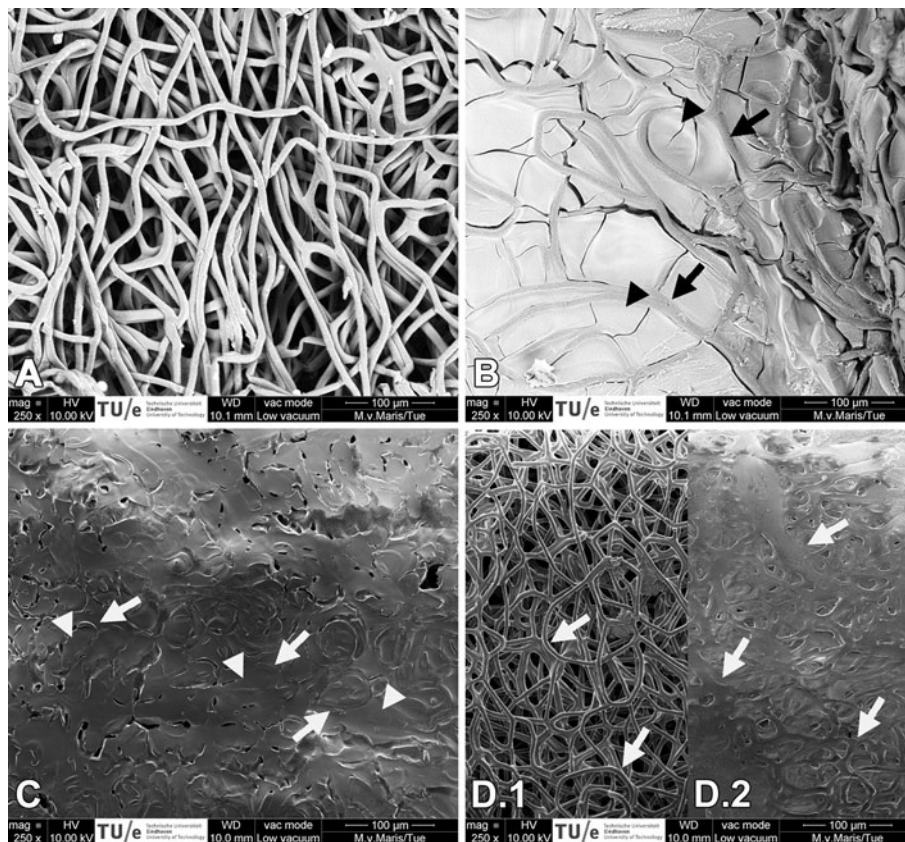

FIGURE 4. SEM image of a native/control, solder-soaked, irradiated solder-soaked, MB-soaked scaffold, and irradiated MB-soaked scaffold. (a) SEM image of native PCL scaffold as control, showing layers of intertwined fibers. (b) SEM image of the solder-soaked scaffold showing solder (arrowheads) filling the area between the intact PCL fibers (arrows). (c) SEM analysis after dual-pass irradiation of solder-soaked scaffold demonstrated a coagulated solder layer (arrowheads) that coalesced with the PCL fibers (arrows). (d) Alteration of PCL fiber structure following dual-pass laser irradiation was evident in the irradiated-MB soaked scaffold (d.2). Fibers were found melted and heterogeneously sized (d.2, arrows), which was in contrast with the homogenously sized fibers in the MB-soaked scaffold (d.1, arrows).
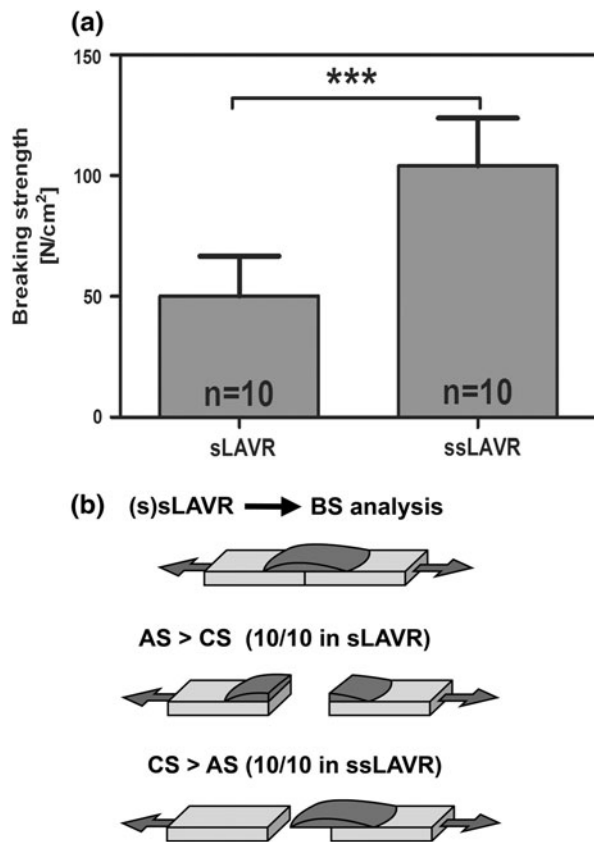
FIGURE 5. (a) Breaking strength in the sLAVR (control) group compared to the ssLAVR group. (b) Schematic drawing of the type of breaking during breaking strength measurements (top image); cohesive failure is defined as the type of break in which the coagulated solder fractured at the incision line with the solder remaining attached to the tissue surface (middle image), whereas adhesive failure is defined as the type of break in which the coagulated solder (and scaffold) remained intact, but the welded strips failed by a complete detachment of scaffold and solder from the opposite tissue surface (bottom image).

difficulties in laser dosing, sLAVR should be strictly employed to seal suture gaps and puncture wounds rather than as a means to make anastomoses in medium- and large-sized vessels. With the advent of polymeric scaffolds as reinforcement material in sLAVR, this statement may in fact become out-dated. In this study, we have shown that the combination of sLAVR with electrospun PCL scaffold material yielded high supraphysiological LPPs in medium-sized arteries (0.37–0.70 cm), albeit in a vessel diameter-dependent manner, without notable structural damage beyond the lower tunica media. The fortification of the weld emanated from the coalescence between melted PCL fibers and denatured solder proteins, which led to an increase in mechanical strength and a simultaneous decrease in elasticity. Correspondingly, the weak point of the weld was located at the solder–tissue interface,

where the fortifying properties of PCL have no influence.

After first having established the optimum welding parameters for PCL ssLAVR,[23] the dependence of LPP on arterial diameter was investigated in this study to assess the potential applicability of PCL ssLAVR for a class of blood vessels previously deemed ill-suited for sLAVR, namely medium-sized vessels.[3] Although the negative correlation between LPP and arterial diameter reflects a restricted range of vessel diameters suitable for ssLAVR, the LPPs (484 ± 111 mmHg) remained well above malignant hypertension levels (systolic blood pressure of 220 mmHg) for vessels with an external diameter of up to 0.70 cm. Provided that porcine arteries used in this study are anatomically comparable to medium-sized arteries in adult humans, e.g., the coronary,[35] internal carotid,[14] renal,[1] and brachial artery,[10] our results are encouraging in regard to the possibility of performing sutureless laser-mediated anastomoses in medium-sized vessels in the clinical setting. Furthermore, the currently obtained LPPs are significantly higher than reported for PLGA-enhanced sLAVR (300 mmHg),[19] underscoring the pivotal role of PCL as a novel biomaterial for ssLAVR with respect to welding strength.

Mechanical tests in substudy IV evinced that the twofold increase of BS in the ssLAVR group (vs. the sLAVR group) was accompanied by a shift from cohesive to adhesive failure, indicating that the scaffold-mediated enhancement of the solder's cohesive strength exceeded the strength of the protein cross-links at the solder–tissue interface. In solid-solder sLAVR, for example, the weakness of the adhesive bond is considered a major disadvantage[26] inasmuch as it annuls the strength benefits offered by the reinforcement through cohesive bonds.[27] Consequently, numerous approaches have been devised to improve adhesive bonding, including (1) confinement of heat delivery to the solder–tissue interface by applying the solder and scaffold separately,[18] employment of a dual-layered solid solder with (2) a chromophore gradient[20] or (3) a film of solder composed of a white layer of solid albumin and a layer of black carbon,[16] (4) using an intraluminal laser source,[6] (5) minimizing solder leakage by modified solder application techniques,[27] and (6) addition of a protein cross-linker to the solder mixture.[15]

The last two approaches, namely the reduction of solder leakage and the use of a protein linker, are effective, practical, and easily applicable. A means to minimize solder leakage, recently introduced by Bleustein et al.,[5] encompasses the addition of hydroxypropylmethylcellulouse to liquid albumin solder, resulting in a semi-solid albumin solder. The high viscosity of the semi-solid solder successfully reduced

solder leakage and significantly increased BS following *in vitro* and *in vivo* laser welding of intestinal tissue and skin, respectively.[5] The use of a semi-solid solder to reduce solder leakage can facilely be combined with a protein cross-linker to improve adhesive strength. A protein cross-linker such as genipin has two aldehyde groups that can be exploited to cross-link the albumin to adventitial collagen during (s)sLAVA/R.[16] Our future studies will therefore include both strategies to further optimize the PCL ssLAVR modality for medium-to-large-sized blood vessels.

Next to welding strength, the extent of thermal damage constitutes an important parameter in laser tissue welding insofar as the retention of viable tissue following laser irradiation is required for an optimal healing process. Despite the difference in arterial diameter, the variation in wall thickness was negligible. Thermal damage in all five samples was found up to 2/3 of the medial layer. In the presence of transmural damage, an intact internal elastic lamina and endothelium after LAVR have been associated with a normal healing response and the deterrence of intimal hyperplasia.[11,29,31,36] In light of these reports, a proper healing process can thus be expected for PCL ssLAVR, where the post-irradiation damage profile was characterized by limited medial damage and an uncompromised internal elastic lamina and endothelial layer. With respect to the adventitial layer, the thermal damage profile suggests that the temperature during ssLAVR resided between the denaturation temperature of collagen (63–75 °C)[17,30] and elastin (120 °C),[13] given the intact state of the elastin fibers. Although the endothelial layer appeared unaffected by the lasing procedure, it should be noted that morphological investigations cannot unequivocally attest to the vitality of endothelial cells and that complete certainty can only be gained in an *in vivo* implantation study.

Transmural thermal damage also induces thinning and hardening of the vascular wall that may bear detrimental clinical consequences. Coagulated albumin solder, which had coalesced with disintegrated and shrunken PCL fibers, had reduced scaffold elasticity and hence contributed to an additional increase in vascular stiffness. Clinically, a constricted and rigidified vascular wall gives rise to compliance mismatch between the stenotic and the non-stenotic distal segment. Such compliance mismatch has been associated with an increase risk of aneurysm formation.[8,32] Consequently, next to the improving adhesive bonding, future research efforts should be focused on minimizing thermal damage and vascular wall stiffness. Prior studies minimized thermal damage by using an intraluminal laser source[6] and by altering the state of the solder (from liquid to solid albumin solder).[21] The retained mechanical strength following welding indicates that PCL might still be a suitable material for ssLAVR from the perspective of welding strength. However, the shrinkage of PCL after ssLAVR remains a concern. Therefore, our future study will also focus on exploring elastic polymers with a higher melting point to reduce scaffold shrinkage during ssLAVR.

CONCLUSIONS

This study demonstrated that PCL ssLAVR of medium-to-large sized arteries yielded high welding strengths in the diameter range of 0.37–0.70 cm in a vessel diameter-dependent manner, whereby thermal damage was confined to the tunica adventia and media. The fortifying effect of the PCL scaffold in ssLAVR resulted in a shift from cohesive to adhesive failure of the weld (vs. sLAVR). The study identified points for further optimization of the ssLAVR modality, including the improvement of adhesive strength, further reduction of collateral thermal damage, and the use of polymers with a higher melting temperature.

ACKNOWLEDGMENTS

OPEN ACCESS

REFERENCES

[1]Aytac, S. K., H. Yigiy, T. Sancak, and H. Ozcan. Correlation between the diameter of the main renal artery and the presence of an accessory renal. Sonographic and angiographic evaluation. *J. Ultrasound Med.* 22:433–439, 2003.

[2]Balguid, A., A. Mol, M. H. van Marion, R. A. Bank, C. V. C. Bouten, and F. Baaijens. Tailoring fiber diameter in electrospun poly(ε-caprolactone) scaffolds for optimal cellular infiltration. *Tissue Eng. Part A* 11:437–444, 2008.

[3]Bass, L. S., and M. R. Treat. Laser tissue welding: a comprehensive review of current and future clinical applications. *Lasers Surg. Med.* 17:315–349, 1995.

[4]Basu, S., S. Wang, R. Robertazzi, P. E. Grubbs, I. Jacobowitz, D. Rose, A. J. Acinapura, and J. N. Cunningham, Jr. In vitro bursting strength studies of laser-welded tissue and comparison with conventional anastomosis. *J. Vasc. Surg.* 7:420–422, 1998.

[5]Bleustein, C. B., C. N. Walker, D. Felsen, and D. P. Poppas. Semi-solid albumin solder improved mechanical properties for laser tissue welding. *Lasers Surg. Med.* 27:140–146, 2000.

[6]Bregy, A., S. Bogni, V. J. Bernau, I. Vajtai, F. Volbach, A. Petri-Fink, M. Constantinescu, H. Hofmann, M. Frenz, and M. Reinert. Solder doped polycaprolactone scaffold enables reproducible laser tissue soldering. *Lasers Surg. Med.* 40:716–725, 2008.

[7]Dalsing, M. C., C. S. Packer, P. Kueppers, S. L. Griffith, and T. E. Davis. Laser and suture anastomosis: passive compliance and active force production. *Lasers Surg. Med.* 12:190–198, 1992.

[8]Demaria, R. G., F. M. Lhote, M. M. Dauzat, M. C. Oliva-Lauraire, J. M. Juan, H. Vernhet, T. Aymard, P. A. Chaptal, and G. Godlewski. Arterial wall compliance after diode laser assisted microanastomosis: a comparative study with conventional manual microanastomosis on rabbit femoral artery. *Lasers Med. Sci.* 15:207–213, 2000.

[9]Fahner, P. J., M. M. Idu, D. A. Legemate, E. van Bavel, J. Borstlao, M. Pfaffendorf, J. van Marle, and T. M. van Gulik. Morphological and functional alteration in glycerol preserved rat aorta allograft. *Int. J. Artif. Organs* 27:979–989, 2004.

[10]Giannattasio, C., M. R. Rivolta, M. Failla, A. A. Mangonit, M. L. Stella, and G. Mancia. Large and medium sized artery abnormalities in untreated and treated hypothyroidism. *Eur. Heart J.* 18:1492–1498, 1997.

[11]Godlewski, G., J. M. Frapier, B. De Balmann, H. Mouzayek, S. Rouy, J. Tang, F. Weible, J. M. Juan, and M. Dauzat. Diode laser and microvascular carotid anastomosis. *Lasers Med. Sci.* 8:33–38, 1993.

[12]Godlewski, G., S. Rouy, J. Tang, M. Dauzat, F. Chambettaz, and R. P. Salathe. Scanning electron microscopy of microarterial anastomoses with diode laser: comparison with conventional manual suture. *J. Reconstr. Microsurg.* 11:37–41, 1995.

[13]Kakivaya, S. R., and A. J. Hoeve. The glass point of elastin. *Biophysics* 72:3505–3507, 1975.

[14]Krejza, J., M. Arkuszewski, S. E. Kasner, J. Weigele, A. Ustymowicz, R. W. Hurst, B. L. Cucchiara, and S. R. Messe. Carotid artery diameter in men and women and the relation to body and neck size. *Stroke* 36:1103–1105, 2006.

[15]Lauto, A., L. J. Foster, L. Ferris, A. Avolio, N. Zwaneveld, and L. A. Poole-Warren. Albumin-genipin solder for laser tissue repair. *Lasers Surg. Med.* 35:140–145, 2004.

[16]Lauto, A., I. Kerman, M. Ohebshalon, D. Felsen, and D. P. Poppas. Two-layer film as a laser soldering biomaterial. *Lasers Surg. Med.* 25:250–256, 1999.

[17]Lemole, G. M., R. R. Anderson, and S. DeCoste. Preliminary evaluation of collagen as a component in the thermally induced 'weld'. *Proc. SPIE* 422:116–122, 1991.

[18]McNally, K. M., B. S. Sorg, E. K. Chan, A. J. Welch, J. M. Dawes, and E. R. Owen. Optimal parameters for laser tissue soldering: II. Premixed versus separated dye-solder techniques. *Lasers Surg. Med.* 26:346–356, 2000.

[19]McNally, K. M., B. S. Sorg, D. X. Hammer, D. L. Heintzelman, D. E. Hodges, and A. J. Welch. Improved vascular tissue fusion using new light-activated surgical adhesive on a canine model. *J. Biomed. Opt.* 6:68–73, 2001.

[20]McNally, K. M., B. S. Sorg, and A. J. Welch. Novel solid protein solders designs for laser-assisted tissue repair. *Lasers Surg. Med.* 27:147–157, 2000.

[21]McNally, K. M., B. S. Sorg, A. J. Welch, J. M. Dawes, and E. R. Owen. Photothermal effects of laser tissue soldering. *Phys. Med. Biol.* 44:983–1002, 1999.

[22]Ott, B., M. A. Constantinescu, D. Erni, A. Banic, T. Schaffner, and M. Frenz. Intraluminal laser light source and external solder: in vivo evaluation of a new technique for microvascular anastomosis. *Lasers Surg. Med.* 35:312–316, 2004.

[23]Pabittei, D. R., M. Heger, R. Balm, H. E. H. Meijer, B. A. deMol, and J. F. Beek. Electrospun poly(ε-caprolactone) scaffold for suture-free solder-mediated laser-assisted vessel repair. *Photomed. Laser Surg.* doi:10.1089/pho.2010.2779.

[24]Pham, Q. P., U. Sharma, and A. G. Mikos. Electropsun poly(epsilon-caprolactone) microfiber and multilayer nanofiber/microfiber scaffolds: characterization of scaffolds and measurement of cellular infiltration. *Biomacromolecules* 7:2796–2805, 2006.

[25]Riley, J. N., T. J. Dickson, D. M. Hou, P. Rogers, K. L. March, and K. M. McNally-Heintzelman. Improved laser-assisted vascular tissue fusion using light-activated surgical adhesive in a porcine model. *Biomed. Sci. Instrum.* 37:451–456, 2001.

[26]Sorg, B. S., K. M. McNally, and A. J. Welch. Biodegradable polymer film reinforcement of an indocyanine green-doped liquid albumin solder for laser-assisted incision closure. *Lasers Surg. Med.* 27:73–81, 2000.

[27]Sorg, B. S., and A. J. Welch. Laser-tissue soldering with biodegradable polymer films in vitro: film surface morphology and rehydration effects. *Lasers Surg. Med.* 28:297–306, 2001.

[28]Sung, H. J., C. Meredith, C. Johnson, and Z. S. Galls. The effect of scaffold degradation rate on three-dimensional cell growth and angiogenensis. *Biomaterials* 25:5735–5742, 2004.

[29]Tang, J., G. Godlewski, S. Ruoy, and G. Delacretaz. Morphological changes in collagen fibers after 830 nm diode laser welding. *Lasers Surg. Med.* 21:438–443, 1997.

[30]Theodossiou, T., G. S. Rapti, V. Hovhannisyan, E. Georgiou, K. Politopoulos, and D. Yova. Thermally induced irreversible conformational changes in collagen probed by optical second harmonic generation and laser-induced fluorescence. *Lasers Surg. Sci.* 17:34–41, 2002.

[31]Unno, N., S. Sakaguchi, and K. Koyano. Microvascular anastomosis using a new diode laser system with a contact probe. *Lasers Surg. Med.* 9:160–168, 1989.

[32]White, A. J., S. J. Duffy, A. S. Walton, S. Mukherjee, J. A. Shaw, G. L. Jennings, A. M. Dart, and B. A. Kingwell. Compliance mismatch between stenotic and distal reference segment is associated with coronary artery disease instability. *Atherosclerosis* 206:179–185, 2009.

[33]Wolf-de Jonge, I. C., J. F. Beek, and R. Balm. 25 Years of laser-assisted vascular anastomosis (LAVA): what have we learned? *Eur. J. Vasc. Endovasc. Surg.* 27:466–476, 2004.

[34]Wolf-de Jonge, I. C., M. Heger, J. van Marle, R. Balm, and J. F. Beek. Suture-free laser-assisted vessel repair using

CO_2 laser and liquid albumin solder. *J. Biomed. Opt.* 13:044032, 2008.

[35]Zindrou, D., K. M. Taylor, and J. P. Bagger. Coronary artery size and disease in UK South Asian and Caucasian men. *Eur. J. Cardiothorac. Surg.* 29:492–495, 2006.

[36]Zubilewicz, T., J. Wronski, A. Bourriez, P. Terlecki, A. M. Guinault, B. Muscateli-Groux, J. Michalak, D. Melliere, J. P. Becquemin, and E. Allaire. Injury in vascular surgery-the intimal hyperplastic response. *Med. Sci. Monit.* 7:316–324, 2001.